On the computation of steady hopper flows I: stress determination for Coulomb materials.[1]

Pierre A. Gremaud and John V. Matthews

Department of Mathematics and Center for Research in Scientific Computation, North Carolina State University, Raleigh, NC 27695-8205, USA

E-mail: gremaud@math.ncsu.edu, jvmatthe@eos.ncsu.edu

The problem of determining the steady state flow of granular materials in silos under the action of gravity is considered. In the case of a Mohr-Coulomb material, the stress equations correspond to a system of hyperbolic conservation laws with source terms and boundary conditions. A higher order Discontinuous Galerkin method is proposed and implemented for the numerical resolution of those equations. The efficiency of the approach is illustrated by the computation of the stress fields induced in silos with sharp changes of the wall angle.

Key Words: granular flow; plasticity; hyperbolic conservation laws; discontinuous Galerkin

1. INTRODUCTION

This is the first of a series of papers in which we study and implement numerical methods for the computation of granular flows. The long term goal is the efficient and reliable numerical simulation of the flow of granular materials in containers and silos, under the action of gravity. Some of the corresponding points under study, discussed in more details below, are

- stress and velocity determination for steady flows (Mohr-Coulomb materials),
- stress, velocity and density determination for steady flows (other types of materials),
- determination and prediction of general flow patterns (mass flow vs. funnel flow),
- application to industrial problems (flow optimization),
- construction, study and resolution of acceptable time dependent models.

This paper deals with the stress determination of the steady state flow of Mohr-Coulomb materials under gravity in axisymmetric containers.

The handling of granular materials is of the greatest importance for many manufacturing industries, where vast quantities of raw materials are stored and handled in granular form.

[1] This research was supported by the Army Research Office (ARO) through grants DAAH04-95-1-0419, DAAH04-96-1-0097 and DAAD19-99-1-0188, by the National Science Foundation (NSF) through grant DMS-9818900, and by a grant from the North Carolina Supercomputing Center.

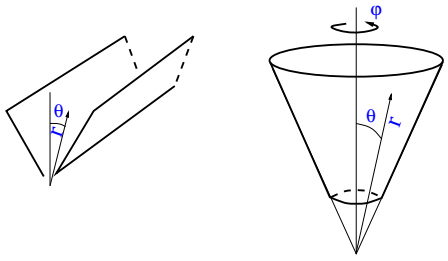

wedge-shaped hopper conical hopper

FIG. 1. Geometry and coordinate systems for the two-dimensional, wedge-shaped hopper and the three-dimensional conical hopper.

Problems of interest can range from applications in the Chemical and Pharmaceutical Industries involving only a few grams of material to large installations holding several thousand tons in the Mining Industry. Serious difficulties during the withdrawal process are often observed. Those range from dead zones of materials sticking to the container's walls and flow stoppage to violent vibrations that can cause the complete collapse of the structure. None of those phenomena is fully understood. An improvement with respect to the understanding and predictability of those effects would hopefully help to reduce the huge financial losses that routinely result from the above problems.

In spite of wide ranging applications going from the above industrial problems to soil mechanics for instance, the *modeling* of granular materials has not reached a level of maturity that is anywhere near what has been achieved in Fluid Mechanics for instance. The culprit is found in the fact that *friction*, a poorly understood concept on its own, is for most regimes the governing phenomenon. Indeed, the properties of a granular material lie between those of a liquid and those of a solid. This can be illustrated by noticing that, even at rest, a granular material can sustain some shearing stress, but only in an amount proportional to the "average stress". When, and only when, the upper limit is reached, the material *yields*, i.e., some deformation takes place. Various yield conditions have been proposed, among them the Mohr-Coulomb yield condition and the von Mises yield condition [8]. The first one is the granular counterpart of the Tresca yield surface found in the Theory of plastic flows of metals, while the second one is, not surprisingly, the analog of a von Mises condition. In the absence of any compelling experimental evidence pointing to one model rather than the other [8], p.290, as being the "best", the yield condition used here is of the Mohr-Coulomb type. The reason for this choice is simplicity since in that case the steady state equations are always hyperbolic (they can sometimes switch to elliptic with a von Mises condition [14]) and the stress equations decouple from the velocity equations. The latter of course still contain the stress, see Section 2; under a von Mises condition no decoupling takes place.

Apart from the choice of a plasticity model, the two main physical assumptions, discussed in Section 2, are first that only established steady state flows are considered and second, that the material is assumed to be everywhere at yield. Most of the existing work in this field deals with steady state flows in conical (or wedge-shaped) hoppers, i.e., when using spherical coordinates, in domains such as

$$\{(r, \theta, \varphi); r > 0, 0 \leq \theta < \theta_w, 0 \leq \varphi \leq 2\pi\},$$

which corresponds to an infinite, converging hopper of half opening angle θ_w, see Figure 1.

In this work, both two-dimensional wedge-shaped hoppers and three-dimensional conical ones are considered. The attention devoted to those cases stems from two reasons. First, in a great number of applications, the containers are indeed axisymmetric, if not downright piecewise conical. Second, as a consequence of the invariance of the domain under the scaling transformation $(r, \theta, \varphi) \mapsto (\lambda r, \theta, \varphi)$ where $\lambda > 0$, similarity solutions, the so-called *radial solutions*, can be constructed. This was first observed by Jenike [6], and has played a fundamental role in the design of industrial hoppers ever since [8], [12]. The radial solutions can be found numerically by solving systems of ordinary differential equations, specifically, boundary value problems. Their behavior is well documented, see e.g. [4], [9] or Section 4. Numerical comparisons of radial fields for both Mohr-Coulomb and von Mises models can be found in [4] and [8].

In this paper, we focus on the stress equations. The corresponding steady state equations representing balance of forces are found to form a hyperbolic system of conservation laws with several nonstandard features. For instance the yield condition by itself does not lead to a properly defined flux, but is rather an additional algebraic constraint, see Section 2. More precisely, using the symmetry of the problem, it is possible to bring the number of unknown components of the stress tensor down to three, while conservation of momentum yields two nontrivial equations (both in the two and three dimensional cases). The plasticity model is what links the three unknowns together and closes the system. This forces the three dependent variables to stay on a manifold: the yield surface, which for the present Mohr-Coulomb materials is a cone, see Figure 2 below. One way to accommodate this is through an additional physical assumption: *realization of passive rather than active states*, see [8] and Section 2. This is the point of view taken here. It has the advantage of keeping the system in conservation form, but does restrict somewhat the range of applicability, see Section 6. Another point of view consists in "solving" the constraint through a clever reparameterization of the surface: use of the so-called *Sokolovskii variables*. This is the standard approach, see again Section 6 and the references given there. However, it comes at the heavy price of destroying the conservation form of the equations, and can thus only be trusted for the calculations of smooth stress fields. The approach taken here allows for the reliable calculations of shock waves for instance. Finally, aside from friction between the grains, from which stem the above plasticity models, another important aspect of the problems at hand is friction between the grains and the container's walls. An application of the law of sliding friction yields boundary conditions that complete the hyperbolic system.

The outline of the paper is as follows. Modeling issues are discussed in Section 2. A brief analysis of the resulting equations is given in Section 3. Section 4 is devoted to the study of similarity solutions. The algorithm and numerical difficulties are discussed in Section 5. Finally, numerical results are presented and commented in Section 6 which is followed by concluding remarks in Section 7.

2. THE MODEL

The equations governing the *time dependent* flow of granular material under gravity are derived and analyzed in [14]. Those are found to be linearly illposed in most cases of practical interest. To the authors' knowledge, the situation is not fully understood, mathematically or otherwise. In practice, strongly time-dependent problems are usually observed in conjunction with *funnel flows*, i.e., flows for which the motion is essentially restricted to the central part of the silo. This paper deals exclusively with *mass flows*, i.e.,

flows for which all the material is mobilized. In this context, established, steady state flows can be observed.

The spatial domain is taken to be axisymmetric, but not necessarily right conical. The particles are assumed to have no motion in the axial (or φ) direction. Even though this assumption may be counterintuitive to fluid dynamicists, it is an established experimental fact for granular materials. The dependent variables reduce to four components of stress and two of velocity:

$$T = \begin{bmatrix} T_{rr} & T_{r\theta} & 0 \\ T_{r\theta} & T_{\theta\theta} & 0 \\ 0 & 0 & T_{\varphi\varphi} \end{bmatrix} \qquad v = \begin{bmatrix} v_r \\ v_\theta \\ 0 \end{bmatrix}. \tag{1}$$

The equations of motion are

$$\nabla \cdot T = \rho g, \qquad \nabla \cdot v = 0, \tag{2}$$

in which ρ is the density, taken to be constant, and the vector g is the acceleration due to gravity. The first equation represents the balance of forces in the material, while the second expresses incompressibility.

The assumption of a constant density deserves some comments. In some practical situations, for instance near the outlet of a hopper, the bulk density may decrease to levels where the particles are no longer in sustained contact with each other. This is the case if the material, on leaving the silo, goes into free fall. However, most industrial silos are equipped with some type of feeder devices that reduce the output rate to values much less than free fall. Note also that failing this, neglecting the inertia terms as we did in (2) would probably not be justified; see [8] on those questions. The treatment of low density granular flows, which is not covered here, can be approached through kinetic or mixed frictional-kinetic theories for granular materials, see [7] and the references therein.

Plastic deformation is assumed everywhere. Constitutive models based on plasticity are conveniently expressed in terms of the principal stresses $\sigma_i, i = 1, 2, 3$, i.e., the eigenvalues of the stress tensor T. If the principal stresses are ordered $\sigma_1 \geq \sigma_2 \geq \sigma_3$, then the *Mohr-Coulomb* yield condition takes the form

$$\frac{\sigma_1}{\sigma_3} = \frac{1 + \sin\delta}{1 - \sin\delta}, \tag{3}$$

where δ is the angle of internal friction. This relation can be derived from the law of sliding friction [8], Chap. 3. By introducing an "average" stress $q = \frac{1}{2}(\sigma_1 + \sigma_3)$, one can easily rewrite the yield condition as

$$(\sigma_1 - q)^2 + (\sigma_3 - q)^2 = 2\, q^2 \sin^2\delta.$$

Further, this condition can be expressed in the original stress variables

$$(T_{rr} - T_{\theta\theta})^2 + 4\, T_{r\theta}^2 = \sin^2\delta\, (T_{rr} + T_{\theta\theta})^2. \tag{4}$$

Additional constitutive assumptions are needed to close the systems. In the Mohr-Coulomb analysis, σ_2 does not appear. The *Haar-von Karman* assumption can be invoked to

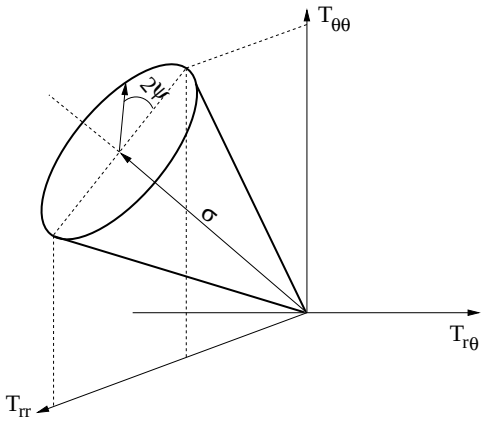

FIG. 2. Plasticity model: the Mohr-Coulomb yield surface.

evaluate the circumferential stress $T_{\varphi\varphi}$. Indeed, the Mohr-Coulomb analysis merely states $\sigma_1 \geq T_{\varphi\varphi} \geq \sigma_3$. For axisymmetric converging hoppers, the Haar-von Karman assumption states that $T_{\varphi\varphi}$ is in fact the major principal stress, i.e., $T_{\varphi\varphi} = \sigma_1 = q\,(1+\sin\delta)$. The *flow rule*, which relates the stress to the deformation through the *strain rate tensor*, defined as (note the sign convention)

$$
\begin{aligned}
V &= -\frac{1}{2}(\nabla v + (\nabla v)^T) \\
&= \begin{bmatrix} -\partial_r v_r & (-\frac{1}{r}\partial_\theta v_r - \partial_r v_\theta + \frac{v_\theta}{r})/2 & 0 \\ (-\frac{1}{r}\partial_\theta v_r - \partial_r v_\theta + \frac{v_\theta}{r})/2 & -\frac{1}{r}(\partial_\theta v_\theta + v_r) & 0 \\ 0 & 0 & -\frac{v_r \sin\theta + v_\theta \cos\theta}{r \sin\theta} \end{bmatrix}
\end{aligned}
$$

is taken according to the *principle of coaxiality*. In other words, the stress tensor T and the strain rate tensor V are assumed to have parallel eigenvectors.

One can gather the above observations in the following system

$$
\begin{gathered}
\partial_r T_{rr} + \tfrac{1}{r}\,\partial_\theta T_{r\theta} + \tfrac{2\,T_{rr}}{r} + \tfrac{\cot\theta}{r}\,T_{r\theta} - \tfrac{1}{r}\,(T_{\theta\theta} + T_{\varphi\varphi}) = -\rho g\cos\theta \\
\partial_r T_{r\theta} + \tfrac{1}{r}\,\partial_\theta T_{\theta\theta} + \tfrac{3}{r}\,T_{r\theta} + \tfrac{1}{r}\cot\theta\,(T_{\theta\theta} - T_{\varphi\varphi}) = \rho g\sin\theta \\
(T_{rr} - T_{\theta\theta})^2 + 4\,T_{r\theta}^2 = \sin^2\delta\,(T_{rr} + T_{\theta\theta})^2 \\
T_{\varphi\varphi} = \tfrac{1}{2}(T_{rr} + T_{\theta\theta})(1+\sin\delta) \\
\partial_r v_r + \tfrac{1}{r}\,\partial_\theta v_\theta + \tfrac{2}{r}\,v_r + \tfrac{1}{r}\,\cot\theta\,v_\theta = 0 \\
\left(\partial_r v_r - \tfrac{\partial_\theta v_\theta}{r} - \tfrac{v_r}{r}\right)\tfrac{2\,T_{r\theta}}{T_{rr}-T_{\theta\theta}} - \left(\partial_r v_\theta + \tfrac{\partial_\theta v_r}{r} - \tfrac{v_\theta}{r}\right) = 0.
\end{gathered}
\tag{5}
$$

Therefore, under the above assumptions, the stress equations decouple from the velocity equations (the latter are still coupled to the stresses). Concentrating here exclusively on the stress components, one can write the corresponding equations in terms of two unknowns T_{rr} and $T_{r\theta}$

$$
\begin{aligned}
\partial_\tau T_{rr} - \partial_\theta T_{r\theta} &= f(\tau,\theta,T_{rr},T_{r\theta}) \\
\partial_\tau T_{r\theta} - \partial_\theta T_{\theta\theta} &= g(\tau,\theta,T_{rr},T_{r\theta})
\end{aligned}
\tag{6}
$$

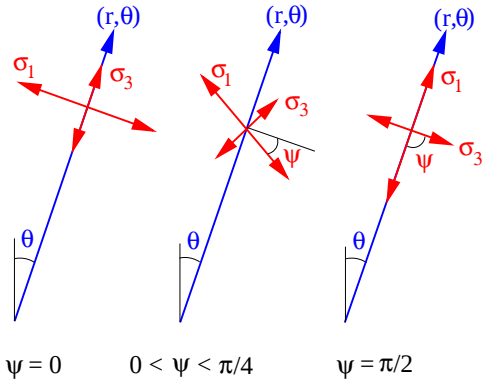

FIG. 3. Physical meaning of the Sokolovskii variable ψ.

where some simplifications result from the use of the new variable $\tau = -\ln r$; we do not bother to rename the stress variables. The right hand side terms are given by

$$\begin{aligned} f(\tau,\theta,T_{rr},T_{r\theta}) &= \tfrac{3-s}{2}\,T_{rr} + \cot\theta\,T_{r\theta} - \tfrac{3+s}{2}\,T_{\theta\theta} + \rho g\,e^{-\tau}\cos\theta \\ g(\tau,\theta,T_{rr},T_{r\theta}) &= -\tfrac{1+s}{2}\cot\theta\,T_{rr} + 3\,T_{r\theta} + \tfrac{1-s}{2}\cot\theta\,T_{\theta\theta} - \rho g\,e^{-\tau}\sin\theta \end{aligned} \tag{7}$$

where we have set $s = \sin\delta$ and, for future reference, $c = \sqrt{1-s^2} = \cos\delta$. The equation of state, which relates $T_{\theta\theta}$ to the unknowns T_{rr} and $T_{r\theta}$ is the yield condition (4). It should be noticed that (4) is the equation of a cone in the space $(T_{rr}, T_{r\theta}, T_{\theta\theta})$, see Figure 2.

The corresponding relation between $T_{\theta\theta}$ and the unknowns is therefore not a proper functional relation, but rather assigns the dependent variables $(T_{rr}, T_{r\theta})$ together with $T_{\theta\theta}$ to lie on a manifold: the yield surface defined by (4). Figure 2 suggests the use of a seemingly more appropriate parameterization of the cone in terms of the Sokolovskii variables (σ, ψ) [8]. The relationship between the two sets of variables is then

$$\begin{aligned} T_{rr} &= \sigma(1 - s\cos 2\psi), & T_{\theta\theta} &= \sigma(1 + s\cos 2\psi), \\ T_{r\theta} &= -\sigma s \sin 2\psi, & T_{\varphi\varphi} &= \sigma(1+s). \end{aligned} \tag{8}$$

It is possible to rewrite the stress equations (6) in terms of the Sokolovskii variables. This approach is quite popular in the present field [8] and was for instance taken in [9], [13] as well as in [10] where more involved models, including compressible flows, are discussed. However, the use of this nonlinear change of variables has the unfortunate side effect of destroying the conservation form of the equations, losing in this way the ability to compute shocks in any reliable way. This would prevent us, for instance, from computing stresses occurring at the junction between conical hoppers of different wall angles, a situation for which discontinuities are to be expected. Further, as is well known, many purely numerical problems also appear when solving systems in nonconservation form.

The Sokolovskii variables are nevertheless valuable in at least two respects. First, as explained next, they admit a useful physical interpretation. Second, in the case of *smooth* flows, see Section 4, they lead to significant mathematical simplifications. In the present axisymmetric setting, the variable ψ is the angle between the position vector at a given point and the direction of the minor principal stress at that point, see Figure 3. The values $|\,\psi\,| \leq \pi/4$ correspond to the so-called *passive* state, [8], [10], as opposed to the *active*

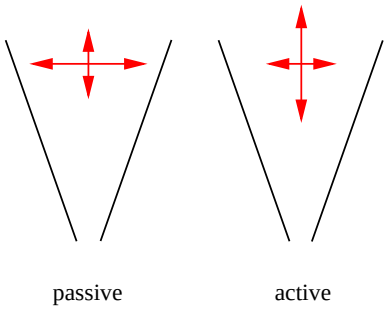

FIG. 4. Difference between passive and active states.

state for which $\frac{\pi}{4} < |\,\psi\,|$. Indeed, the yield condition (3) only prescribes the ratio $\frac{\sigma_1}{\sigma_3}$, but does not differentiate between the two situations of Figure 4.

For converging hoppers, the passive state is the one observed experimentally upon discharge [12], and corresponds to the "top" of the yield surface: a large lateral compression takes place. Going back to the original variables to keep the system in conservation form, one can solve (4) for $T_{\theta\theta}$, and find the equation of state completing (6, 7)

$$T_{\theta\theta} = h(T_{rr}, T_{r\theta}) \equiv \frac{1+s^2}{1-s^2}\,T_{rr} + 2\sqrt{\frac{s^2}{(1-s^2)^2}\,T_{rr}^2 - \frac{1}{1-s^2}\,T_{r\theta}^2}. \tag{9}$$

However, as illustrated in Figure 5, the range of values that can be treated this way is strictly smaller than that of the passive case. One can solve for $T_{\theta\theta}$ as above only if $|\,\frac{T_{r\theta}}{T_{\theta\theta}}\,| < \tan\delta$, which corresponds to $|\,\psi\,| < \frac{\pi}{4} - \frac{\delta}{2}$. The existence of the threshold $\frac{\pi}{4} - \frac{\delta}{2}$ results from our choice of coordinates. By using other coordinate systems, it may be possible to increase the range of values that can be treated by our approach; see further remarks in the next section.

Finally, if instead of a three-dimensional conical hopper, one considers a "two-dimensional" wedge-shaped hopper [7], [8], [9], [10], see Figure 1, the equations simplify to

$$\begin{gathered}
\partial_r T_{rr} + \tfrac{1}{r}\,\partial_\theta T_{r\theta} + \tfrac{1}{r}\,(T_{rr} - T_{\theta\theta}) = -\rho g\cos\theta \\
\partial_r T_{r\theta} + \tfrac{1}{r}\,\partial_\theta T_{\theta\theta} + \tfrac{2}{r}\,T_{r\theta} = \rho g\sin\theta \\
(T_{rr} - T_{\theta\theta})^2 + 4\,T_{r\theta}^2 = \sin^2\delta\,(T_{rr} + T_{\theta\theta})^2 \\
\partial_r v_r + \tfrac{1}{r}\,\partial_\theta v_\theta + \tfrac{1}{r}\,v_r = 0 \\
\left(\partial_r v_r - \tfrac{\partial_\theta v_\theta}{r} - \tfrac{v_r}{r}\right)\tfrac{2T_{r\theta}}{T_{rr}-T_{\theta\theta}} - \left(\partial_r v_\theta + \tfrac{\partial_\theta v_r}{r} - \tfrac{v_\theta}{r}\right) = 0.
\end{gathered} \tag{10}$$

As before, the stress equations decouple and can again be written under form (6) with here

$$\begin{aligned}
f(\tau,\theta,T_{rr},T_{r\theta}) &= T_{rr} - T_{\theta\theta} + \rho g\,e^{-\tau}\cos\theta \\
g(\tau,\theta,T_{rr},T_{r\theta}) &= 2T_{r\theta} - \rho g\,e^{-\tau}\sin\theta
\end{aligned} \tag{11}$$

The systems (5) and (10) have to be completed with appropriate boundary conditions. A brief analysis of the stress equations, presented in the next section, will reveal what kind of boundary conditions leads to well-posedness. The principal parts corresponding to the two and three dimensional problems (10) and (5) being identical, the analysis covers both cases.

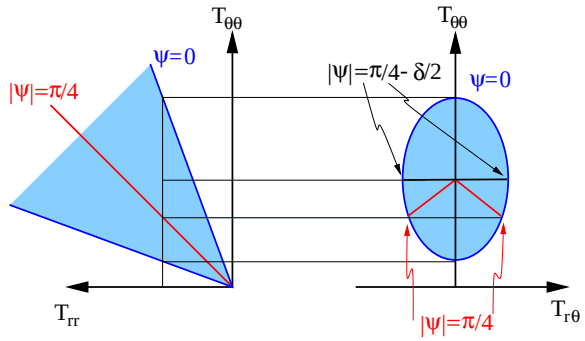

FIG. 5. Illustration of the passive state $|\psi| < \pi/4$ vs. the values for which hyperbolicity is satisfied $|\psi| < \frac{\pi}{4} - \frac{\delta}{2}$, see also Section 3.

3. BRIEF ANALYSIS OF THE EQUATIONS

The stress equations (6) can be rewritten as

$$\partial_\tau U + \partial_\theta F(U) = G, \tag{12}$$

with the obvious notation. One can then analyze the eigenvalues $\lambda_{1,2}$ of the Jacobian F'. A few calculations lead to

$$\lambda_{1,2} = \mp \tan\delta \mp \frac{1}{c}\sqrt{\frac{s\,T_{rr} \mp c\,T_{r\theta}}{s\,T_{rr} \pm c\,T_{r\theta}}}, \qquad r_{1,2} = \begin{bmatrix} 1 \\ \lambda_{1,2} \end{bmatrix}, \tag{13}$$

where $r_{1,2}$ are the corresponding eigenvectors. The eigenvalues are real provided that one stays "in the cone", i.e., $|\frac{T_{r\theta}}{T_{rr}}| < \tan\delta$, which corresponds to the domain of definition of F in (12). In that case, one clearly has $\lambda_1 < \lambda_2$. Consequently, the steady state stress equations (6, 7, 9) form a *strictly hyperbolic system of nonlinear conservation laws with source terms*. The radial and angular variables τ and θ can be thought of as time-like and space-like variables, respectively. One cannot overemphasize the importance of this key observation: the problem of the determination of the stress field is one of *propagation*. Incidentally, it should be noticed that if a von Mises yield surface, [5], [8], is used, instead of the present Mohr-Coulomb approach, then the corresponding three-dimensional steady state equations are sometimes elliptic instead [14]. In the two-dimensional case, both approaches are identical. Numerical comparisons between the two types of models, in the case of similarity solutions, see §4, can be found in [4] and [8].

Additional facts can be uncovered about the hyperbolic system (6) governing the stresses under the present approach. First, the eigenvalues are unbounded, even for bounded stress components. Indeed, for T_{rr} fixed, one observes that

$$\begin{array}{ll} \lambda_1 \longrightarrow -\tan\delta & \text{when } T_{r\theta} \uparrow \tan\delta\, T_{rr}, \\ \lambda_1 \longrightarrow -\infty & \text{when } T_{r\theta} \downarrow -\tan\delta\, T_{rr}, \\ \lambda_2 \longrightarrow \infty & \text{when } T_{r\theta} \uparrow \tan\delta\, T_{rr}, \\ \lambda_2 \longrightarrow \tan\delta & \text{when } T_{r\theta} \downarrow -\tan\delta\, T_{rr} \end{array}$$

Further, direct calculations show that for any $\{T_{rr}, T_{r\theta}\}$ such that $|\frac{T_{r\theta}}{T_{rr}}| < \tan\delta$, one has $\nabla\lambda_i \cdot r_i \neq 0$, $i = 1, 2$. Both characteristic fields are thus genuinely nonlinear.

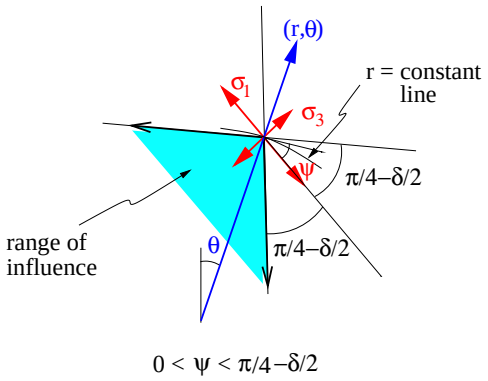

FIG. 6. Link between a possible loss of hyperbolicity and the choice of a coordinate system.

Again, it is instructive to rewrite the expression (13) for the eigenvalues in terms of the Sokolovskii variables (σ, ψ). One finds after some manipulations

$$\lambda_{1,2} = \cot(\psi \mp (\pi/4 - \delta/2)). \tag{14}$$

In other words, the stress characteristics are inclined at $\pm(\pi/4+\delta/2)$ to the major principal stress direction [8], [9], see Figure 6. As noticed in the previous section, values for which $|\psi| \geq \pi/4 - \delta/2$ lead to grief, here through the fact that the range of influence would be partially pointing "into the past" (increasing values of r). One also observes from Figure 6 that this problem could be partially alleviated by changing the time-like variable from radial to a variable whose level lines would be closer to being parallel to the local direction of the major principal stress. How to do this in practice is under study.

We now seek what type of discontinuities constitute admissible shocks for the stress equations (6). To determine the Hugoniot loci, a fixed state $(\hat{T}_{rr}, \hat{T}_{r\theta})$ is considered. The Rankine-Hugoniot condition for (6) takes the form

$$\begin{aligned} \tilde{T}_{r\theta} - \hat{T}_{r\theta} &= w(\tilde{T}_{rr} - \hat{T}_{rr}) \\ \tilde{T}_{\theta\theta} - \hat{T}_{\theta\theta} &= w(\tilde{T}_{r\theta} - \hat{T}_{r\theta}) \end{aligned}$$

where w stands for the shock speed, for lack of a better notation, and $\tilde{\ }$ denotes the states to be found. Eliminating w leads to

$$\Big(h(\tilde{T}_{rr}, \tilde{T}_{r\theta}) - h(\hat{T}_{rr}, \hat{T}_{r\theta})\Big)(\tilde{T}_{rr} - \hat{T}_{rr}) = (\tilde{T}_{r\theta} - \hat{T}_{r\theta})^2$$

where $h(\cdot, \cdot)$ is defined in (9). The above equation is essentially equivalent to a general polynomial equation of degree 4 and, as such, does not admit any easy to handle closed form solutions. Making use of the genuine nonlinearity of both fields, admissibility is given by Lax's entropy condition. Consequently, considering the fixed state $\hat{\ }$ as the left state, a discontinuity in the i-th field, $i = 1, 2,$ is admissible only if

$$\hat{\lambda}_i > w > \tilde{\lambda}_i.$$

The situation is illustrated in Figure 7.

The system has to be completed with "initial" and boundary conditions. The boundary conditions are given by the law of sliding friction. At any point on the wall, the magnitude

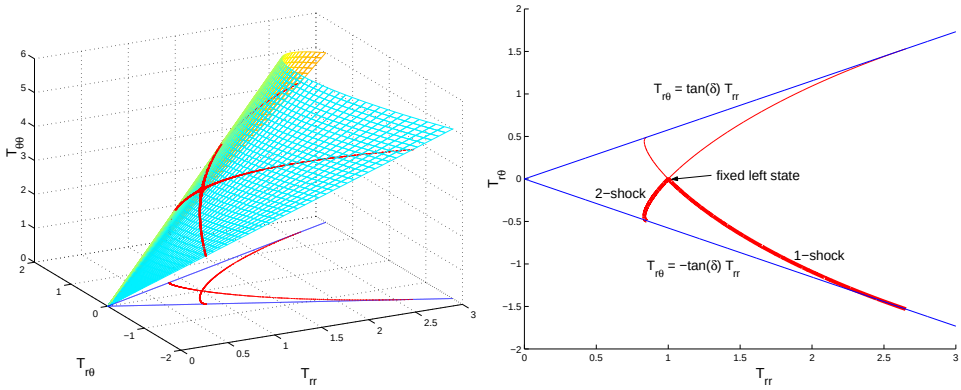

FIG. 7. Hugoniot loci. A fixed state $(\hat{T}_{rr}, \hat{T}_{r\theta}) = (1, 0)$ is considered as the left state. Left: location of the corresponding Hugoniot curves. Right: admissible shocks ($\delta = 30°$).

of the tangential stress $|\, T_T \,|$ is proportional to the magnitude of the normal stress $|\, T_N \,|$, i.e.,

$$|\, T_T \,| = \mu \, |\, T_N \,|,$$

where $\mu > 0$ is the coefficient of wall friction. In a purely radial geometry, the above boundary condition becomes

$$T_{r\theta} = \pm \mu \, T_{\theta\theta} \qquad \text{on the walls} \tag{15}$$

with a "+" sign on one side of the hopper and a "-" sign on the other, see Section 5 for more details.

The case of the "initial" condition is more delicate. It is chosen here to prescribe the stress field high up in the hopper, say, on an "τ = constant" surface, and solve down from there. In other words, it is assumed that stress information flows from the top down, rather than from the bottom up, which would make equal sense mathematically. Indeed, if one puts a weight on top of material in a hopper, stresses increase but the flow speed does not change significantly. On the other hand, if one changes the speed of the flow near the outlet for instance, the velocity field would then change throughout the hopper with only minimal changes in stress. It seems thus that for the full problem (5), velocity information flows from the bottom up [15], see also [17], [18] for some experiment based arguments. Those questions will be the object of future work.

4. SIMILARITY SOLUTIONS

In the early 1960s, Jenike [6] discovered similarity solutions for the steady state equations governing flow of granular materials under gravity in a conical or wedge–shaped hopper. In these solutions, particle paths are radial lines converging to the vertex of the hopper. For this reason, the solutions are referred to as *radial solutions*. The similarity is reflected in scalings of the stress and velocity with respect to radial distance r, with the result that stress decreases along particle paths while the particles accelerate. Radial solutions, tabulated by Jenike for a large range of physical parameters, form the basis for much work on the design of mass flow hoppers [12], in which the flow is thought to be approximately radial. These solutions are also helpful for understanding and studying basic properties of hopper flow [8], and the role of parameters such as internal friction and wall friction.

Following Jenike, one can seek similarity solutions to the two-and three-dimensional problems, respectively (5) and (10), of the form

$$T_{ij}(r,\theta) = r\, T_{ij}(\theta), \qquad v(r,\theta) = -\frac{1}{r^{d-1}} u(\theta) e_r\,,$$

where e_r is the unit vector in the radial direction and d stands for the spatial dimension. The formulation can be simplified through the use of the Sokolovskii variables, see Section 2. Since the similarity solutions sought in this section are smooth, and the use of the Sokolovskii variables is here perfectly justified. The equations defining the radial solutions for the stresses are found to correspond to the following boundary value problem [8], [4]

$$\mathcal{A} \begin{bmatrix} \sigma'(\theta) \\ \psi'(\theta) \end{bmatrix} = \mathcal{B}_d(\theta, \sigma(\theta), \psi(\theta)), \qquad \theta \in (-\theta_w\,, \theta_w\,), \tag{16}$$

$$\psi(\pm\theta_w) = \pm\psi_w\,. \tag{17}$$

In the above problem, the quantities $\mathcal{A}$, $\mathcal{B}_d$, $d = 2$ or 3 and ψ_w are given by

$$\begin{aligned}
\mathcal{A} &= \begin{bmatrix} -s\sin 2\psi & -2s\,\sigma\cos 2\psi \\ 1 + s\cos 2\psi & -2s\,\sigma\sin 2\psi \end{bmatrix}, \\
\mathcal{B}_2(\theta,\sigma,\psi) &= \rho g \begin{bmatrix} -\cos\theta \\ \sin\theta \end{bmatrix} + \sigma \begin{bmatrix} 3s\cos(2\psi) - 1 \\ 3s\sin(2\psi) \end{bmatrix}, \\
\mathcal{B}_3(\theta,\sigma,\psi) &= \rho g \begin{bmatrix} -\cos\theta \\ \sin\theta \end{bmatrix} + \sigma \begin{bmatrix} 4s\cos(2\psi) - 1 + s + s\cot\theta\sin(2\psi) \\ 4s\sin(2\psi) - s(\cos(2\psi) - 1)\cot\theta \end{bmatrix}, \\
\psi_w &= \frac{1}{2}\left(\Phi + \arcsin\left(\frac{\sin\Phi}{s}\right)\right),
\end{aligned}$$

where Φ is the *angle of wall friction*, which is defined by $\tan\Phi = \mu$, $0 \le \Phi \le \pi/2$. The boundary value problem (16) is nonsingular provided that

$$|\,\psi\,| < \frac{\pi}{4} + \frac{\delta}{2}.$$

Note that the above is a third critical value of $|\,\psi\,|$, in addition to the first two discussed in Figure 5 which corresponded respectively to the threshold hyperbolic/non-hyperbolic and passive/active. The fact that the problem of finding the radial fields may become singular under some circumstances should not come as a surprise. Indeed, the assumption that the material is at yield everywhere, which precludes the formation of rigid areas in the flow, is clearly not satisfied if the opening angle is too wide.

The above problem (16) has to be solved numerically. This can easily be done through the use of a collocation method for instance, such as COLSYS [1] that was used here and is based on collocation at Gaussian points. A study of the properties and stability of radial solutions can be found in [4], see also [8] and [9] for earlier results.

5. THE ALGORITHM

For the sake of simplicity, we only describe the algorithm in the case of a conical hopper. The method used is a formally high order Discontinuous Galerkin scheme, see [3] and the references listed therein.

Let $\tau_0 = -\ln r_0$, where r_0 is the value of the radial variable we start from. Let $\theta_w > 0$ be the half opening angle, and let $\Delta\theta = \theta_w/N$ be the mesh size, N being the number of cells. In this axisymmetric setting, the problem is essentially one-dimensional "spatially", and thus no efforts have been made to adapt the mesh. We define

$$V = \{v \in L^\infty(0,\theta_w)^2 : v|_{K_j} \in P^k(K_j)^2, j = 0,\ldots,N-1\},$$

where $K_j = [\,\theta_{j-1/2}, \theta_{j+1/2}\,]$ is the j-th cell, with $\theta_{j-1/2} = j\,\Delta\theta$, and $P^k(K_j)$ stands for the space of the polynomials of degree at most k in K_j. We use $k = 1$ or 2 below; see §6. A semidiscretization consists in looking for $U_h(\tau,\cdot) \in V$, $\tau > \tau_0$, such that $U_h(\tau_0,\cdot) = \Pi_V(U(\tau_0,\cdot))$, where $U(\tau_0,\cdot)$ is an "initial condition", see §6, Π_V is a projection operator into V, and

$$\begin{aligned}\frac{d}{d\tau}\int_{K_j} & U_h(\tau,\theta)\,v(\theta)\,d\theta + \Delta_+\left(v(\theta_{j-1/2})\,H_{j-1/2}\right)\\ &- \sum_{l=1}^{5}\omega_l F(U_h(\tau,\theta_{j,l}))\,\frac{d}{d\theta}v(\theta_{j,l})\Delta\theta\\ &= \sum_{l=1}^{5}\omega_l G(\tau,\theta_{j,l},U_h(\tau,\theta))\,v(\theta_{j,l})\Delta\theta, \qquad \forall v\in V, j=1,\ldots,N.\end{aligned}$$

In the previous expression, Δ_+ stands for the usual difference operator, $\Delta_+ U_j = U_{j+1} - U_j$ and the coefficients ω_l and the nodes $\theta_{j,l}$, $l = 1,\ldots,5$, $j = 1,\ldots,N$ stem from the use the classical 5-point Gaussian quadrature formula. We use the local Lax-Friedrichs flux

$$H_{j+1/2} = \frac{1}{2}\left(F(U^-_{j+1/2}) + F(U^+_{j+1/2}) - \alpha_{j+1/2}(U^+_{j+1/2} - U^-_{j+1/2})\right),$$

where $\alpha_{j+1/2}$ is the magnitude of the largest eigenvalue of a properly chosen Roe average matrix $A_{j+1/2} \approx (\frac{dF}{dU})_{U=U_{j+1/2}}$ [11]. Rewriting the equation of state (9) as $h(a,b) = \alpha\,a + \sqrt{\beta a^2 + \gamma b^2}$, with $\alpha = \frac{1+s^2}{1-s^2}$, $\beta = \frac{4s^2}{(1-s^2)^2}$ and $\gamma = \frac{-4}{1-s^2}$, the Roe average matrix $A_{j+1/2}$ can be chosen here as

$$A_{j+1/2} = -\begin{bmatrix} 0 & 1 \\ \alpha + \beta\frac{\bar a_{j+1/2}}{\bar\chi_{j+1/2}} & \gamma\frac{\bar b_{j+1/2}}{\bar\chi_{j+1/2}}\end{bmatrix},$$

where the averages are defined by $\bar a_{j+1/2} = (a^-_{j+1/2} + a^+_{j+1/2})/2$, $\bar b_{j+1/2} = (b^-_{j+1/2} + b^+_{j+1/2})/2$ and $\bar\chi_{j+1/2} = \sqrt{\beta(a^-_{j+1/2})^2 + \gamma(b^-_{j+1/2})^2}/2 + \sqrt{\beta(a^+_{j+1/2})^2 + \gamma(b^+_{j+1/2})^2}/2$.

The mass matrix can be made diagonal by choosing the basis functions as Legendre polynomials over each cell [2]. The coefficients of $U_h(\tau,\cdot)$ can then be grouped in a vector $\mathcal{U}(\tau)$. The unknown vector $\mathcal{U}(\tau)$ satisfies the following system of ODEs

$$\frac{d}{d\tau}\mathcal{U} = \mathcal{F}(\mathcal{U}) + \mathcal{G}(\tau,\mathcal{U}) \tag{18}$$

where $\mathcal{F}(\mathcal{U})$ and $\mathcal{G}(\tau,\mathcal{U})$ come respectively from the discretization of $F(U)$ and $G(\tau,\theta,U)$ in (12). Note that we use below an unsplit approach. This is justified first by the fact that the source term $\mathcal{G}(\tau,\mathcal{U})$ is not stiff and second, by the realization that the delicate interplay

between $\mathcal{G}(\tau, \mathcal{U})$ and the boundary conditions would render the implementation of a split algorithm a lot more involved than the present approach.

The discretization with respect to τ involves a third order TVD Runge-Kutta [16] combined with a local slope limiting process. Let $\Delta\tau > 0$ be a constant increment in τ and let $\tau^n = \tau_0 + n\Delta\tau$ and N_τ be the number of time steps. The algorithm reads then as follows, see e.g. [3]

- Set $U^{(0)} = \Lambda\Pi(U_h(\tau_0, \cdot))$;
- For $n = 0, \ldots, N_\tau - 1$, compute U_h^{n+1}:
  1. set $U^{(0)} = U_h^n$;
  2. for $i = 1, \ldots, 3$, compute the intermediate stages

$$U^{(i)} = \Lambda\Pi \left(\sum_{j=0}^{i-1} \alpha_{ij} U^{(j)} + \Delta\tau\, \beta_{ij} \left(\mathcal{F}(U^{(j)}) + \mathcal{G}(\tau^n + d_j \Delta\tau, U^{(j)}) \right) \right);$$

  3. set $U_h^{n+1} = U^{(3)}$.

The numerical parameters $\{\alpha_{ij}\}$, $\{\beta_{ij}\}$ and $\{d_j\}$, $i = 1, 2, 3$, $j = 0, 1, 2$ are respectively defined as

$$\begin{array}{lll} 1 & & \\ 3/4 & 1/4 & \\ 1/3 & 0 & 2/3 \end{array} \qquad \begin{array}{lll} 1 & & \\ 0 & 1/4 & \\ 0 & 0 & 2/3 \end{array} \qquad \begin{array}{l} 0 \\ 1 \\ 1/2 \end{array}$$

A thorough description of the local slope limiting operator $\Lambda\Pi$, which is based on the use of a corrected minmod function, can be found, e.g., in [3] (see [2] for the modifications to $\Lambda\Pi$ at the boundary); it is not repeated here. Note that both $\Lambda\Pi$ and the proper implementation of the boundary conditions (15) require transformation to the characteristic fields.

The construction of the numerical flux at the boundaries deserve some comments. Expressed in the original variables, the boundary conditions are

$$T_{rr} \text{ even}, \quad T_{r\theta} \text{ odd at} \quad \theta = 0,$$

and

$$T_{r\theta} = -\mu T_{\theta\theta} \quad \text{at} \quad \theta = \theta_w\,.$$

The corresponding nodes are $\theta_{-1/2} = 0$ and $\theta_{N-1/2} = \theta_w$. Considering first the condition at $\theta = \theta_w$, the matrix $A_{N-1/2}$ is diagonalized, $A_{N-1/2} = R\Lambda R^{-1}$, where the columns of $R = [r_1 \,|\, r_2]$ are the right eigenvectors of $A_{N-1/2}$ and $\Lambda = diag(\lambda_1, \lambda_2)$. We know from §3 that $\lambda_1 < 0$ and $\lambda_2 > 0$. The vector $T = \begin{bmatrix} T^-_{rr,N-1/2} \\ T^-_{r\theta,N-1/2} \end{bmatrix}$ is transformed to characteristic variables by left multiplying by R^{-1}, i.e. $\begin{bmatrix} u^-_{1,N-1/2} \\ u^-_{2,N-1/2} \end{bmatrix} = R^{-1}T$. Since $\lambda_2 > 0$, we set $u^+_{2,N-1/2} = u^-_{2,N-1/2}$. The boundary condition $T_{r\theta} = -\mu T_{\theta\theta}$ is used to define $u^+_{1,N-1/2}$. It should be noted that even though the above boundary condition appears to be nonlinear in $(T_{rr}, T_{r\theta})$, it is in fact a linear relation. This can be seen geometrically since this amounts to taking the intersection of the yield cone (4), see Figure 2, by a

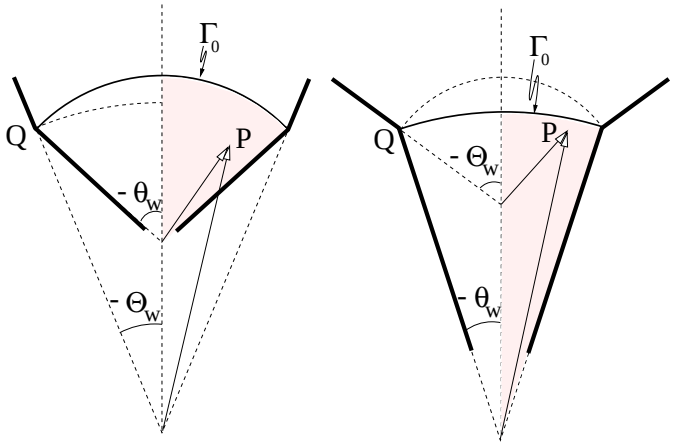

FIG. 8. Geometrical situation; left: transition to a flatter wall angle, right: transition to a steeper wall angle. The radial stress is used to generate an initial condition on the curve Γ_0. The domains of calculation are shaded.

plane $T_{r\theta} = -\mu T_{\theta\theta}$ through the vertex of the cone. Algebraically, the boundary condition reduces to

$$T_{rr} = \chi_w T_{r\theta} \qquad \text{with } \chi_w = -\frac{1 - s\cos 2\psi_w}{s \sin 2\psi_w},$$

where ψ_w is defined as in (16). By translating this condition to characteristic variables through $R = [r_1 | r_2]$, one obtains

$$u^+_{1,N-1/2} = \frac{-r_{12} + \chi_w r_{22}}{r_{11} - \chi_w r_{21}} u^+_{2,N-1/2}.$$

The values entering as arguments in the numerical flux at $\theta = \theta_w$ are then

$$\begin{bmatrix} T^+_{rr,N-1/2} \\ T^+_{r\theta,N-1/2} \end{bmatrix} = R \begin{bmatrix} u^+_{1,N-1/2} \\ u^+_{2,N-1/2} \end{bmatrix}.$$

The conditions are $\theta = 0$ simply correspond the symmetry properties of the stress components and are directly implemented as

$$\begin{bmatrix} T^-_{rr,-1/2} \\ T^-_{r\theta,-1/2} \end{bmatrix} = \begin{bmatrix} T^+_{rr,-1/2} \\ -T^+_{r\theta,-1/2} \end{bmatrix}.$$

6. COMPUTATIONAL RESULTS

We analyze the influence of abrupt changes in the wall angle on the stress field. The geometrical situation is illustrated in Figure 8.

Any point P admits two representations, namely, (R, Θ) and (r, θ), corresponding to the natural coordinate systems for the upper and lower hopper respectively. The transition is located through the point Q, see again Figure 8, where $Q = (R_0, -\Theta_w) = (r_0, -\theta_w)$. For given values of the material parameters δ and μ, the numerical approach consists then of

- generating the radial stress field T in the upper hopper $\{(R, \Theta) : R > 0, |\Theta| \leq \Theta_w\}$ [4], [8]; by construction, at a point (R, Θ), the radial stress field is given by $R\,T(\Theta)$;

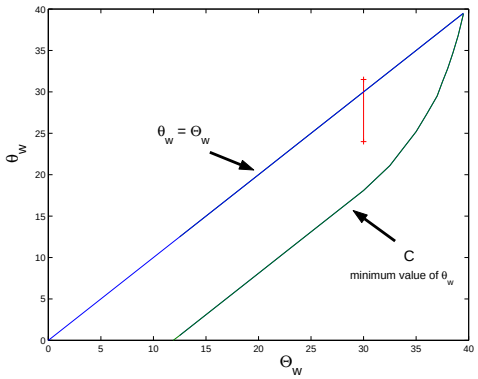

FIG. 9. Range of values of θ_w leading to a well defined "initial" condition for given values of Θ_w; $\delta = 32.1°$, $\mu = \tan(11.7°)$.

- interpolating the radial stress field on the curve $\Gamma_0 = \{(r,\theta) : r = r_0, |\,\theta\,| \leq \theta_w\}$, leading to a stress tensor S_{Θ_w};
- changing to the new coordinate system to get $S_{\theta_w} = \mathcal{R}^T(\Theta-\theta)S_{\Theta_w}\mathcal{R}(\Theta-\theta)$, where $\mathcal{R}(\alpha)$ is the rotation matrix of angle α;
- solving in the lower hopper $\{(r,\theta) : 0 < r < r_0, 0 < \theta < \theta_w\}$ using the algorithm described in §5, and $\mathcal{S}_{\theta_w}$ as an initial condition.

The boundary conditions are implemented as described at the end of the previous section §5.

Some comments are in order. First, the fact that the initial condition is generated from the radial stress field implicitly assumes that this very solution is sought and realized by the problem in the upper part of the hopper. Second, it also takes as granted that the radial solution reaches the curve Γ_0 unperturbed by the wall corner. This last point is clearly satisfied, assuming again a downward propagation of the information for the stresses, in the case of a transition to a flatter hopper, i.e., $\Theta_w < \theta_w$, see Figure 8, left. If the transition is to a steeper hopper, $\theta_w < \Theta_w$, see Figure 8, right, a quick analysis based on the characteristic curves reveals that the difference in angles should not be too large, namely

$$\Theta_w - \theta_w < \arctan\left|\frac{1}{\lambda_{max}}\right|, \qquad \theta_w, \Theta_w > 0.$$

Here λ_{max} is the largest eigenvalue in modulus of F', see (13), evaluated along the curve Γ_0 (an r equal to constant line for the lower hopper).

By way of illustration, we consider $\delta = 32.1°$ and $\mu = \tan(11.7°)$ and determine the maximum transition for a range of upper hopper wall angles, Θ_w, see Figure 9. It is clear from the expression for the eigenvalues in terms of the Sokolovskii variables (14) that the maximum value of ψ determines the eigenvalue of largest modulus and thus the limitation on the size of the transition. First, note that the value of ψ at the wall in the upper hopper is independent of the wall angle Θ_w, see e.g. (16). As can be checked numerically, for the present illustration ψ is monotonic for values of Θ_w up to $22.4°$. Thus for this range of opening angles, its maximum value is found at the wall. Consequently, the maximum transition allowed for $\Theta_w < 22.4°$ is constant. In Figure 9, this corresponds to the linear portion of the curve (marked C) representing the minimum theoretical value of θ_w. For $\Theta_w > 22.4°$, ψ ceases to be monotonic and has a global maximum in the interior of the

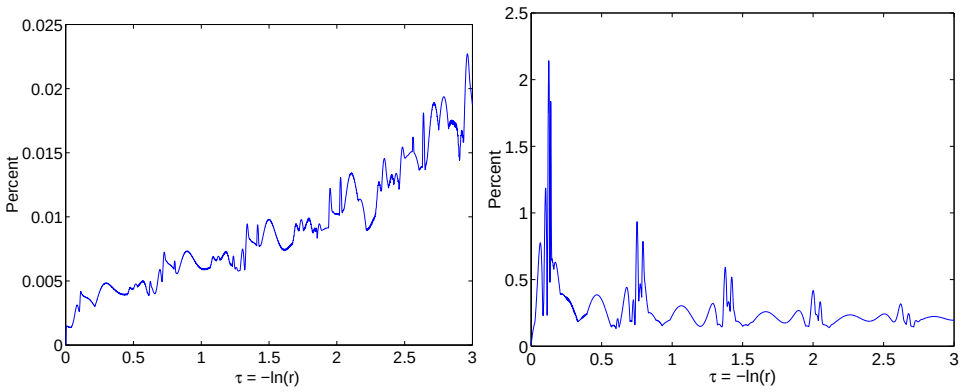

FIG. 10. Preservation of the radial field by the PDE solver. Left: wedge-shaped hopper, right: conical hopper. For each value of $\tau = -\ln r$, the error is represented by the maximum percentage of difference between the radial field and the PDE solution; $\theta_w = \Theta_w = 30°$, $\delta = 32.1°$, $\mu = \tan(11.7°)$.

domain. It can be checked, again through the numerical calculation of the radial field, that the maximum value of ψ keeps increasing as Θ_w is increased further. This results in a decrease in size of the allowable transition. This can be seen by the curve C approaching the line $\theta_w = \Theta_w$. For some value of Θ_w, $39.5°$ for the present example, the maximum transition has neared zero (curve C intersects the line $\theta_w = \Theta_w$) and our current approach cannot treat even the initial condition since there, the maximum of ψ is already greater than $\pi/4 - \delta/2$ and a transition to a hopper of steeper wall angle can only make the problem more difficult.

While determining whether an initial condition fits the limitations of our current approach can be easily done as above, checking whether the problem stays "solvable" for all $\tau > 0$ is not as clear. This amounts to establishing a priori bounds on the magnitude of ψ. This was done a posteriori, and numerically, for the above example. Turning again to Figure 9, the vertical bar at $\Theta_w = 30°$ denotes the actual (small) range of transitions over which the solution can be computed for $\tau >> 0$.

Finally, the case $\theta_w = \Theta_w$ can be used to check that the algorithm effectively preserves the radial solution. The interaction between the boundary conditions and the forcing terms renders this numerically delicate. Further, the radial solution itself may be unstable [4]. For $\theta_w = \Theta_w$, the present approach preserves the radial solution with a great degree of accuracy. In Figure 10, the relative difference between the radial solution at any given "time" τ and the solution from the PDE solver is illustrated. Both graphs in Figure 10 correspond to an integration 95% down the hopper. One observes that even though in both cases the error is quite small, the behaviors of the two-and three-dimensional problems are quite different. For the two-dimensional problem, the largest discrepancy is less than .025%, but it appears to be increasing as one progresses down the hopper. In the three dimensional case, the largest value of the discrepancy is about 100 times larger, but the difference decreases as one solves down the hopper to an asymptotic value less than .5%. The fact that the two-dimensional problem is less stable than its three-dimensional counterpart was already observed in [9], see also [4] for a linear stability study. Because the initial condition is constructed as a projection into polynomial space of a numerical solution, it does not exactly satisfy the boundary conditions. The resulting perturbations propagate through the hopper and are amplified when being reflected at the center, or more precisely when interacting with similar waves coming from across the hopper. In the three-dimensional axisymmetric

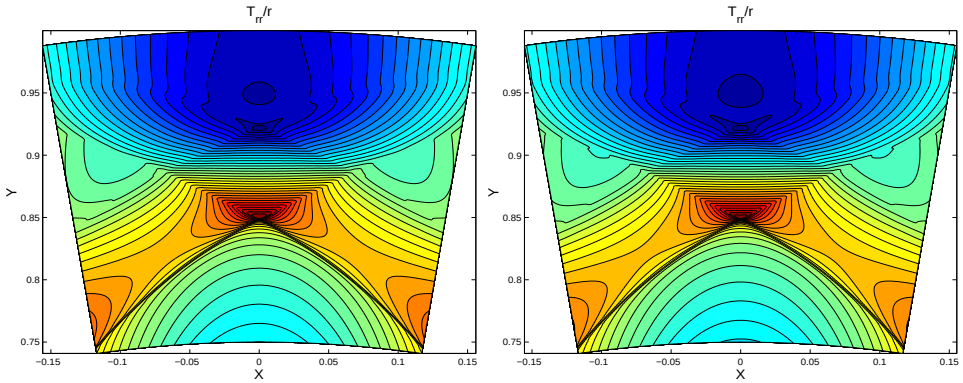

FIG. 11. Details for a transition from a conical $\Theta_w = 30°$ hopper to a $\theta_w = 24°$ one, $\delta = 32.1°$, $\mu = \tan(11.7°)$. Left: P^1 approximation with $N = 400$; right: P^2 approximation with $N = 200$.

case, those waves come from all directions, which is not the case of the two-dimensional problem. The spikes observed in Figure 10, right, correspond the interactions of those waves at the center. Below, both the case of a transition to a steeper hopper, $\theta_w < \Theta_w$, and that of a transition to a shallower one, $\theta_w > \Theta_w$ are considered. One can note that with respect to applications, it may be even more important to treat the flow near the juncture between a *cylindrical* silo and a conical hopper. However, the two cases, i.e., cylindrical vs conical, correspond to two different types of motion. Indeed, in cylindrical geometry, the material can flow without deforming. Further, the state in the cylindrical portion is likely to be active (as a result of the filling process), while the passive state is expected in the converging conical silo, see §2 and [8], [10], [13]. The determination of the precise nature of the transition between the passive and active part of the flow and the corresponding "switch stresses" [8], §7.13 are still to our knowledge essentially open problems. To avoid those delicate problems, we consider here exclusively junctures between two converging conical (or wedge shaped) hoppers, so as to have a passive state throughout. Some predictions as to do what happens can be found in the literature [8], p.237. By invoking a simple characteristics analysis and/or by using a (dangerous) analogy with Fluid Dynamics, one may guess that transitions to steeper hoppers will lead to rarefaction waves formation, while transitions to shallower hoppers should correspond to the formation of shock waves. To some extent, our results confirm this, but also show that the situation is in general far more complex.

The computational results given below for values of the material parameters

$$\delta = 32.1°, \quad \mu = \tan 11.7°, \quad \rho = 790 kg/m^3,$$

which roughly corresponds to corn in a steel hopper. The number of "spatial" cells (angular variable) in the half hopper corresponding the domain of calculation is $N = 400$. The time step (radial increment) is chosen as to satisfy the experimental stability condition [2]

$$\lambda_{max} \frac{\Delta\tau}{\Delta\theta} \leq \frac{1}{2k+1},$$

λ_{max} is the magnitude of the largest eigenvalue all the Roe matrices. Finally, most of the results presented are for a polynomial approximation of degree $k = 1$. Using discontinuous P^2, $k = 2$, did not lead to significant improvements at comparable cost, see Figure 11, and

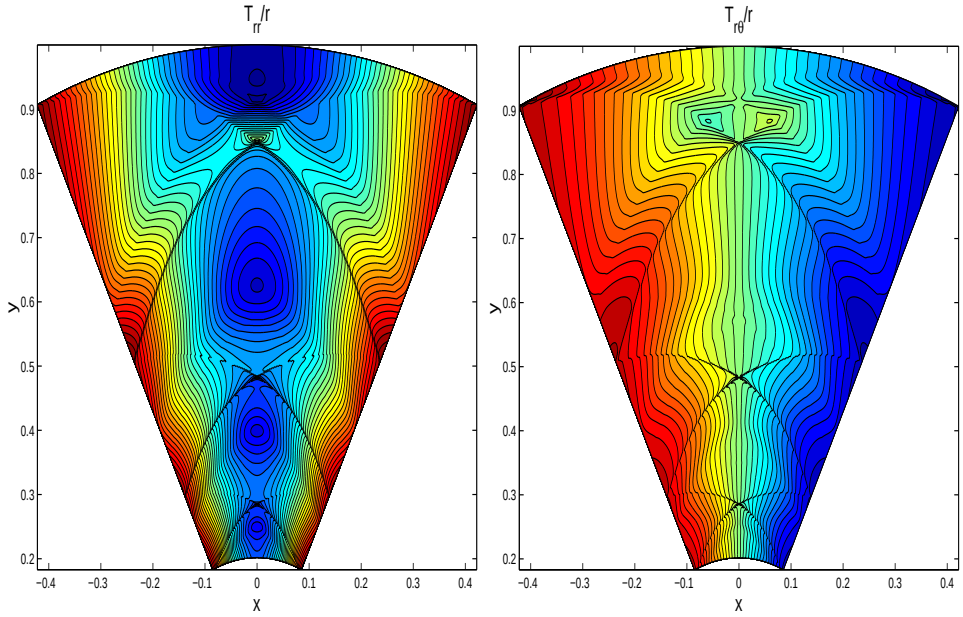

FIG. 12. Transition from a conical $\Theta_w = 30°$ hopper to a $\theta_w = 25°$ one, $\delta = 32.1°$, $\mu = \tan(11.7°)$.

led to more restrictive experimental stability conditions. Note that in Figure11 as well as in all the results below, the stress components are plotted scaled by r, so as to illustrate the convergence, or the lack thereof, to a radial field.

Figure 12 illustrates the effects on the stress field of a transition from a $30°$ conical hopper to a $25°$ one. One can clearly observe the formation of rarefaction waves originating from the line of transition. As one moves down the hopper, those waves converge from all directions to the center of the cone where they interact. This in turn induces a strong sharpening, eventually resulting in shock waves. In spite of this, a slow convergence back to a radial field can also be observed in this case, as well as in all our three-dimensional experiments.

The same transition as above, i.e., $30° \rightarrow 25°$, but from a two-dimensional wedge-shaped hopper is represented in Figure 13. Here as well, there is initial formation of rarefaction waves. In this case the steeping of the waves is slower. However, the main feature here is that the field does not go back to radial as one moves down the hopper. In fact, the periodic like structure that can be observed in Figure 13 is representative of our two-dimensional experiments. Next, we consider transitions from steeper hoppers to shallower ones. For those cases, it turns out that values incompatible with our model, i.e., $|\psi| \geq \pi/4 - \delta/2$ (see above discussion) are very easily reached. This is especially true of the three-dimensional case where transitions of only about $2°$ in the wall angle could be treated. Problems involving this kind of transitions for two-dimensional wedge-shaped hoppers revealed to be more accommodating. Figure 14 illustrates the transition from a $30°$ wedge-shaped hopper to a $35°$ one. This time, one can observe the formation of shock waves emanating from the opening angle transition. Again, a periodic like pattern appears and no transition back to a radial structure is observed.

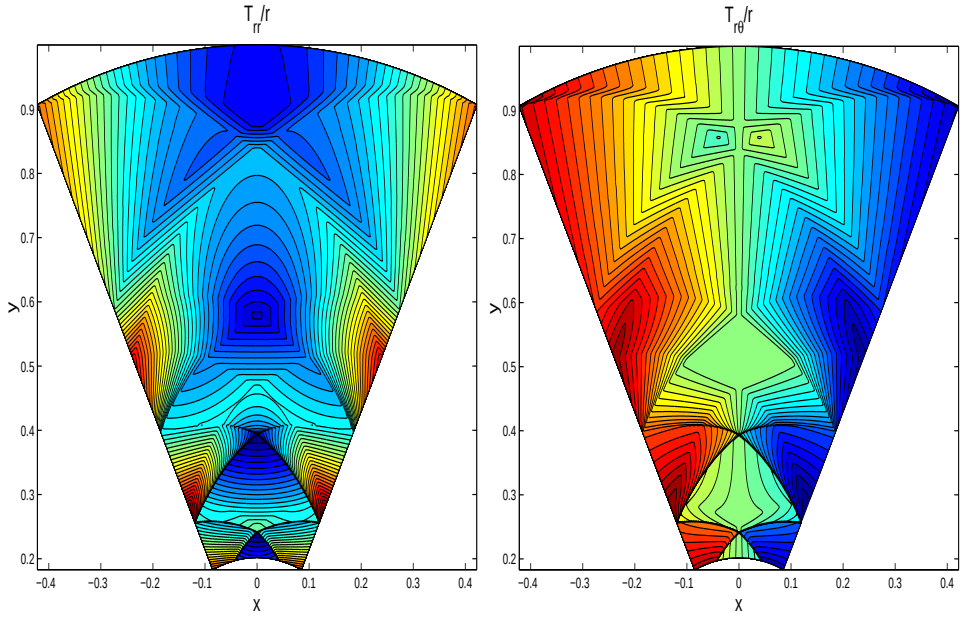

FIG. 13. Transition from a wedge-shaped $\Theta_w = 30^\circ$ hopper to a $\theta_w = 25^\circ$ one, $\delta = 32.1^\circ$, $\mu = \tan(11.7^\circ)$.

7. CONCLUDING REMARKS

The steady state flow of granular materials in silos under the action of gravity is considered. We focus here on Mohr-Coulomb materials for which the equations determining the stress field can be solved independently of the other variables (velocity and/or density). Those equations form a system of hyperbolic conservation laws. The equation of state derives from the plasticity model and does not correspond to a proper functional relation but rather to an algebraic constraint. The standard way around this has been so far the use of a parameterization of the manifold (yield surface) corresponding to the above constraint. How to do this without losing the conservation form of the system is not clear. In other words, this approach can only be used for the calculation of *smooth* stress fields. The point of view taken here is to work directly with the stress components, i.e., *without* a parameterization of the yield surface. As a result, conservation form is preserved, allowing for instance for the reliable calculations of shock waves. The algebraic constraint is "solved" by restricting the type of problems considered. Only flows in the passive state (in fact even only a subset of those) can be treated. However, and unlike the previous work we are aware of, the present approach can be applied the determination of the effects on the stress field of sharp transitions in the opening angle of the hopper containing the material (changes in the physical properties of the walls, i.e., wall friction, can be similarly treated).

The equations are discretized through a Discontinuous Galerkin method. The presence of both boundary conditions and source terms lead to some numerical difficulties and prompted the use of an unsplit implementation. The transition problems from shallower to steeper hoppers are solved successfully by the present approach for a wide range of parameters, this both in the case of three-dimensional conical hoppers and two-dimensional wedge-shaped ones. Transitions from steeper to shallower hoppers are found to be more delicate. While the two-dimensional case can still be efficiently treated, it is found that

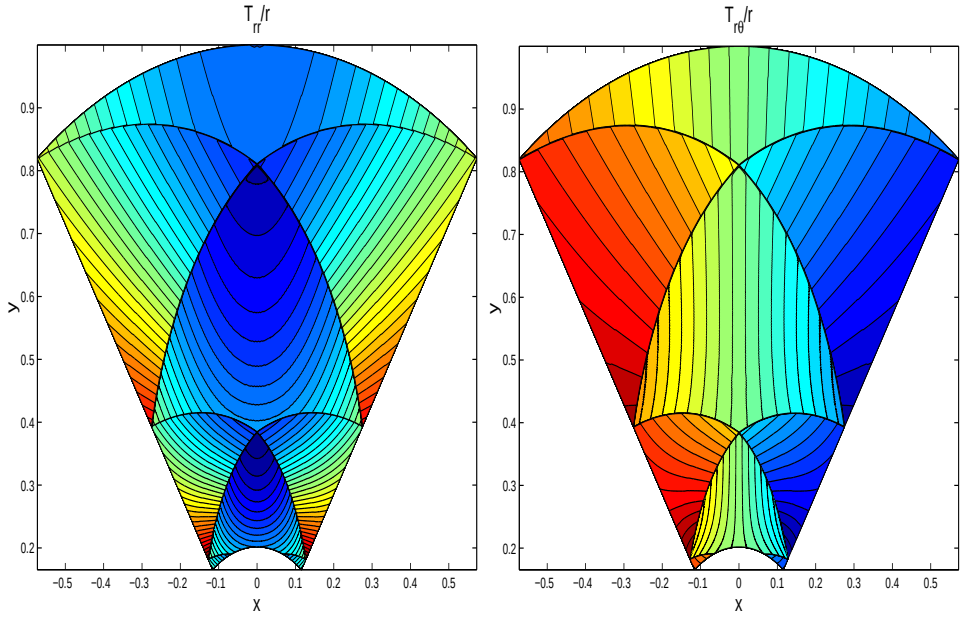

FIG. 14. Transition from a wedge-shaped $\Theta_w = 30^\circ$ hopper to a $\theta_w = 35^\circ$ one, $\delta = 32.1^\circ$, $\mu = \tan(11.7^\circ)$.

three-dimensional hoppers can only accommodate small transitions of this type. This limitation is not physical nor is it related to a short coming of the numerics, but ultimately results from the coordinate system's choice. Roughly speaking, characteristics that should be "pointing down" (decreasing values of the radial time-like variable) stop doing so, resulting in a loss of hyperbolicity. The study of alternate coordinate systems that would expand the range of parameters for which the present method applies while keeping the equations in conservation form is under way.

The resolution of the full problem, i.e., determination of stress and velocity fields, will be the object of a future publication.

ACKNOWLEDGMENT

The authors would like to thank Tony Royal, Dave Schaeffer and Michael Shearer for many helpful discussions.

REFERENCES

1. U. Ascher, J. Christiansen and R. Russel, Collocation software for boundary value ODE's, *ACM Trans. Math. Software*, **7** (1981), p.209–222, http://www.netlib.org/ode/colsys.f
2. B. Cockburn, S.Y. Lin and C.W. Shu, TVB Runge-Kutta local projection discontinuous Galerkin finite element method for conservation laws III: one dimensional systems, *J. Comput. Phys.*, **84** (1989), p.90–113.
3. B. Cockburn and C.W. Shu, The Runge-Kutta discontinuous Galerkin method for conservation laws V: multidimensional systems, *J. Comput. Phys.*, **141** (1998), p.199–224.
4. P.A. Gremaud, J.V. Matthews and M. Shearer, Similarity solutions for granular flows in hoppers, in *Proceedings of the SIAM/AMS Conference on Nonlinear PDEs, Dynamics and Continuum Physics*, edited by J. Bona, K. Saxton, R. Saxton, AMS Contemporary Mathematics Series, 1998, to be published.
5. P.A. Gremaud, D.G. Schaeffer and M. Shearer, Numerical determination of flow corrective inserts for granular materials in conical hoppers, *Int. J. Nonlinear Mech.*, to be published.
6. A. Jenike, Gravity flows of bulk solids, Bulletin No. 108, vol. 52, Utah Eng. Expt. Station, University of Utah, Salt Lake City (1961)

7. R. Jyotsna and K. Kesava Rao, A frictional-kinetic model for the flow if granular materials through a wedge-shaped hopper, *J. Fluid Mech.*, **346** (1997), p.239–270.
8. R.M. Nedderman, *Static and kinematic of granular materials*, Cambridge University Press (1992).
9. E.B. Pitman, The stability of granular flow in converging hoppers, *SIAM J. Appl. Math.*, **48** (1988), p.1033–1052
10. J. Ravi Prakash and K. Kesava Rao, Steady compressible flow of cohesionless granular materials through a wedge-shaped bunker, *J. Fluid Mech.*, **225** (1991), p.21–80
11. P.L. Roe, Approximate Riemann solvers, parameter vectors, and difference schemes, *J. Comp. Phys.*, **43** (1981), p.357–372
12. A.T. Royal, Private communication, Jenike & Johanson, Inc., (1998, 1999).
13. S.B. Savage and R.N. Yong, Stresses developed by cohesionless granular materials in bins, *Int. J. Mech. Sci.*, **12** (1970), p.675–693.
14. D.G. Schaeffer, Instability in the evolution equations describing incompressible granular flow, *J. Diff. Eq.*, **66** (1987), p.19–50.
15. D.G. Schaeffer, Private communication, (1998, 1999).
16. C.W. Shu and S. Osher, Efficient implementation of essentially non-oscillatory shock-capturing schemes, *J. Comp. Phys.*, **77** (1988), p.439–471.
17. U. Tüzün and R.M. Nedderman, Gravity flow of granular materials round obstacles-I: investigation of the effects of inserts on flow patters inside a silo, *Chem. Engng. Sci.*, **40** (1985), p.325–336.
18. U. Tüzün and R.M. Nedderman, Gravity flow of granular materials round obstacles-II: investigation of the stress profiles at the wall of a silo with inserts, *Chem. Engng. Sci.*, **40** (1985), p.337–351.